Physica Medica 108 (2023) 102573

Contents lists available at ScienceDirect

Physica Medica

journal homepage: www.elsevier.com/locate/ejmp

Technical note

Technical note: Simulation of lung counting applications using Geant4

Henri Jutila [a,b,*], Paul Greenlees [a,b], Tiina Torvela [c], Maarit Muikku [c]

[a] Accelerator Laboratory, Department of Physics, University of Jyväskylä, FI-40014 Jyväskylä, Finland
[b] Helsinki Institute of Physics, University of Helsinki, P.O. Box 64, FI-00014 Helsinki, Finland
[c] STUK – Radiation and Nuclear Safety Authority, Jokiniemenkuja 1, FI-01370 Vantaa, Finland

ARTICLE INFO

Keywords:
Lung counting
Voxel phantom
Geant4 simulation
Low-energy gamma-ray spectra

ABSTRACT

A Geant4 simulation package has been developed to investigate and test detector configurations for lung counting applications. The objective of this study was to measure radiation emitted from the human body and to make a qualitative comparison of the results of the simulation with an experiment. Experimental data were measured from a plastic phantom with a set of lungs containing ^{241}Am activity. For comparison, simulations in which ^{241}Am activity was uniformly distributed inside the lungs of the ICRP adult reference computational phantom were made. The attenuation of photons by the chest wall was simulated and from this photopeak efficiency and photon transmission were calculated as a function of photon energy. The transmission of 59.5 keV gamma rays, characteristic of the decay of ^{241}Am, was determined from the computational phantom as a function of the angular position of the detector. It was found that the simulated detector response corresponds well with that from an experiment. The simulated count rate below 100 keV was 10.0(7) % greater compared to the experimental measurement. It was observed that 58.3(4) % of photons are attenuated for energies below 100 keV by the chest wall. In the simulation, the transmission of 59.5 keV gamma rays varied from 13.8(2) % to 38.0(4) % as a function of the angular position of the detector. The results obtained from the simulations show a satisfactory agreement with experimental data and the package can be used in the development of future body counting applications and enables optimization of the detection geometry.

1. Introduction

Ionizing radiation is present everywhere in our environment. An individual's personal annual radiation dose originates from radionuclides in soil, air, food, water, cosmic radiation, medical use of radiation, and other man-made sources. While people are constantly bombarded with ionizing radiation from all directions, it does not generally impose a threat to the health of the public. However, in case of radiation accidents, internally deposited activity, especially inhaled, can be extremely dangerous and can result in a radiation dose many times higher than the normal annual dose. Therefore, it is necessary to have methods to assess the level of internal exposure of the human body and the circumstances of the exposure. The level of exposure can be determined indirectly by measuring environmental samples and fecal or urine samples from the individual or directly using whole body or partial body counters [1].

Lung counting refers to a direct measurement of the inhaled activity contained in the lungs using a set of sensitive scintillation or semiconductor detectors with good energy resolution placed outside the body close to the chest. Even small amounts of radioactive material containing, e.g., americium or plutonium, are extremely dangerous when inhaled due to the long biological half-life [2,3]. These radioisotopes can be released into the environment from nuclear accidents, explosions, nuclear reactors, and from manufactured products that contain such isotopes.

Due to the short range of alpha and beta particles in matter, detection of these particles outside of the body is possible only indirectly, for instance by measuring fecal or urine samples. In order to get reliable results, urine and fecal samples collected during 24-hour and 3–4-day periods respectively, are analyzed [1]. Therefore, it is necessary to resort to the detection of photons for direct measurements. However, observing radionuclides via low-energy gamma-ray detection is difficult. A non-uniform distribution of unknown radionuclides which changes over time after intake makes dose assessment difficult [4]. Most of the low-energy gamma rays with energies below 100 keV are either partially or fully absorbed by the chest wall. In addition, a low-energy background is generated in the region of interest by the Compton scattering of higher energy gamma rays in the detector material and in the body before detection. Typical measurements using current detectors

* Corresponding author at: Accelerator Laboratory, Department of Physics, University of Jyväskylä, FI-40014 Jyväskylä, Finland.
E-mail address: henri.m.jutila@jyu.fi (H. Jutila).

https://doi.org/10.1016/j.ejmp.2023.102573
Received 1 June 2022; Received in revised form 3 February 2023; Accepted 21 March 2023

require a long measurement time and/or a low-background environment, which may not be available in an accident scenario.

Radiation transport codes are extremely important in many fields of research from medical physics to high energy physics. Codes can be used, for example, to optimize the detection of radiation [5], estimate radiation doses [6], and in treatment planning for radiotherapy together with realistic computational phantoms [7]. Widely used codes such as GATE [8], EGSnrc [9], MCNP5 [10], PENELOPE [11], FLUKA [12], and Geant4 [13] are all based on the Monte Carlo method that relies on repeated random sampling to obtain a numerical result.

Based on the Geant4 platform [13], a simulation package for lung counting has been constructed including the International Commission on Radiological Protection (ICRP) adult reference computational phantoms [14] and a simple cylindrical (planar) Hyper-Pure Germanium (HPGe) semiconductor detector. The computational phantoms are based on tomographic data sets. The package converts the phantom data into voxels which have an atomic composition and density defined by the ICRP [14]. The germanium detector has been modeled based on a simplified version of existing detectors used in the whole body counting laboratory at the Radiation and Nuclear Safety Authority (STUK).

The present work aims to confirm the viability of the package as a platform to test and optimize future body counting applications which aim to improve the existing measurement setup at STUK in terms of Minimum Detectable Activity (MDA) and measurement time. The viability is assessed by using Monte Carlo methods to replicate experimental lung counting data, determine the simulated photon transmission and photopeak efficiency as a function of gamma-ray energy, and understand how the geometry of the phantom affects the attenuation of 59.5 keV gamma rays as a function of the angular position of the detector.

2. Material and methods

In the following section, the foundation for the methods used, and definitions of the various parameters employed in the analysis are presented in more detail.

2.1. Photopeak efficiency

The gamma and X-ray activity can be quantified by identifying the characteristic photopeaks and determining the count rate, R, given by the number of recorded events, N, in the peak relative to the measurement time, Δt,

$$R = \frac{N}{\Delta t} \tag{1}$$

The activity can then be determined using the photopeak efficiency η defined as

$$\eta = \frac{R}{AI} \tag{2}$$

where A is the activity of the radioactive source, and I is the fractional yield of a radiation per disintegration or emission intensity. The photopeak efficiency is a dimensionless number but can be expressed as counts in a photopeak/total number of photons emitted by the source. It gives the probability of a given emitted photon to be absorbed by the detector and produce a full-energy peak in the final spectrum.

2.2. Photon transmission

The chest wall, which is composed of bone, cartilage, muscle, and adipose tissue, has a great effect on the low-energy gamma- and X-rays. The attenuation of photons by the chest wall can be investigated and evaluated by determining the probability of photon transmission with Monte Carlo methods. The photon transmission Φ/Φ_0 is defined as the ratio between the photon flux, Φ, after penetrating the absorbing medium and the initial photon flux, Φ_0, emitted from the radiation source. In the present work, the ratio Φ/Φ_0 is defined as the number of events in the photopeak after penetrating the chest wall of the computational phantom divided by the number of events in the photopeak when the computational phantom is not present. Therefore, the coefficient (1 - Φ/Φ_0) represents the number of incident photons that are partially or fully absorbed by the chest wall or other scattering processes within the detector for a specific photon energy. In HPGe detectors, for low photon energies (<140 keV) the photon interactions are dominated by the photoelectric effect rather than Compton scattering. Therefore, at low energies, the Compton background is mostly generated by the scattering of higher energy gamma rays in the chest wall if no other radiation source is present in the simulation.

2.3. Experimental measurement

The experimental data was obtained using a human torso phantom (ARDF-09T), referred to as the physical phantom from now on. It consists of 14 detachable plastic parts including a set of lungs containing ^{241}Am manufactured by STC RADEK, Russia, the physical phantom is shown in Fig. 1a) without the chest plate. The composition of the plastic parts is based on epoxy resin with fillers. The densities of material imitators are 1.056 g/cm^3 and 0.261 g/cm^3 for soft and pulmonary tissues, respectively. The chest plate is contaminated with ^{241}Am and was therefore replaced with a 5.2 kg custom chest plate made from granulated table sugar, mimicking the original, shown in Fig. 1b). Emitted radiation was measured using two S-series HPGe detectors (GEM-S7025P4) manufactured by Ortec, USA. The detectors were rotated towards the middle of the lungs and placed in slight contact with the chest. The left and right lungs with ^{241}Am activities of 19.3 kBq and 23.7 kBq, respectively, were placed inside the phantom and the phantom was placed inside the enclosed low background counting room at STUK. The room is constructed from low-background steel (150 mm) with layers of lead (3 mm) and copper (4 mm) placed on top of special concrete which has 1/8 of the activity concentration of normal concrete. The duration of source measurements was approximately one hour. A background measurement was performed with a similar setup but using lungs that do not contain activity. The duration of the background measurement was around fourteen hours. A DSPEC 502 multichannel analyzer with the Maestro v. 7.01 software package by Advanced Measurement Technology, Inc., USA was used for data acquisition.

2.4. Energy resolution

Gaussian energy broadening [10] was used in the simulation to match the energy resolution of the detector used in the experimental measurement. The energy resolution of a detector system is usually described by the Full Width at Half Maximum (FWHM) which varies as a function of deposited energy, E, and can be expressed in the following form [10]

$$\mathrm{FWHM} = a + b\sqrt{E + cE^2}\ . \tag{3}$$

The FWHM is related to the Gaussian width, σ, by

$$\sigma = \frac{\mathrm{FWHM}}{2\sqrt{2\ln 2}}. \tag{4}$$

Using experimentally determined coefficients a, b, and c, the Gaussian width σ, can be calculated for each deposited photon energy, and matching energy resolution can be achieved by sampling the Gaussian distribution

$$\frac{1}{\sigma\sqrt{2\pi}}\exp\left(-\frac{(x-\mu)^2}{2\sigma^2}\right). \tag{5}$$

a) b)

Fig. 1. a) plastic physical phantom (ARDF-09T) without the contaminated chest plate. b) same physical phantom with a custom chest plate made from granulated table sugar.

2.5. Voxel phantom

ICRP adult reference computational male and female phantoms were used in the lung counting simulation package, the main properties of which are shown in Table 1. The phantoms are based on computed tomography image data of a 38-year-old male (1.76 m, 70 kg) and a 43-year-old female (1.67 m, 59 kg) [14]. Both tomography data sets were segmented, scaled and the tissues adjusted to match the ICRP reference height and total mass [14]. Although the female phantom consists of 348 slices, only 45 slices are used in the simulations which contain the lungs to cut down the computational time. This selection of a smaller number of slices is justified by the small detector frontal area. In the case of the male phantom, only 27 slices are used, since the thickness of a single slice is 8.00 mm, whereas the slice thickness for the female phantom is 4.84 mm. A single slice from both of the phantoms is shown in Fig. 2a) and b) visualized in Geant4. In addition, the arms were removed from the computational phantom in order to determine the variation in count rate as a function of the angular position of the detector.

2.6. Geant4 simulation

The Geant4 (Geometry And Tracking) toolkit for the simulation of the passage of particles through matter [13] (version 10.5) was used to build a lung counting simulation package including voxelized ICRP adult reference computational male and female phantoms [14]. The lung counting simulation package also utilizes parts of the Geant4 simulation package built to simulate the Advanced Gamma Tracking Array (AGATA) [15,16] to generate the output file. Livermore [17] was used as a physics model which describes low-energy interactions for photons and electrons down to 250 eV. Python scripts were used to analyze the simulated data.

Geant4 uses Monte Carlo methods to describe the interaction of particles with matter. In general, Geant4 simulations consist of runs, events, tracks, and steps. By initiating a run, a set of particles are emitted. An event starts when one or more primary particles are generated and consists of the tracks of each particle. A track is a sequence of steps that is defined as the distance between two interaction points. Information about the particle is stored in each step. It is possible, for example, to retrieve the energy deposition during each step, the physical processes involved in the interactions, and the kinetic energy of the particle at the beginning and end of each step [18].

Table 1
Main properties of the ICRP adult reference computational phantoms [14].

Phantom	Male	Female
Height (m)	1.76	1.63
Mass (kg)	73	60
Slice thickness (mm)	8.00	4.84
In-plane resolution (mm)	2.137	1.775
Number of slices	222	348
Number of materials	53	53

The lung counting package requires phantom information specified in the DICOM application of Geant4 [13] and a macro file that contains particle or photon information. At the beginning of an event, random coordinates for the emission point and direction of emission are selected inside the phantom volume. If the material at the emission point is defined to be lung material (other materials besides lung can also be used), the emission of a particle is processed. Otherwise, new coordinates are selected until the material is determined to be lung. Therefore, in the simulation, the activity is uniformly distributed inside the lung or lungs but in reality, this is not the case as discussed in Section 1. However, the small difference in the distribution of the activity within the lungs has no effect on the conclusions of the present work. After a set of pre-determined runs are completed, an output file is generated consisting of the steps of the particles that have interacted inside the detector. By summing the energy deposition after each interaction, a spectrum can be reconstructed and analyzed in the same manner as an experimental spectrum.

A simple cylindrical detector consisting of a germanium crystal inside a vacuum enclosed by an aluminum capsule with a thickness of 1.1 mm and 5.5 mm vacuum space between the crystal and the capsule is used to detect photons emitted from lung voxels, shown in Fig. 2e). The detector is modeled based on an existing planar HPGe detector used in the experimental measurement. The dimensions of the detector are such that it has a radius of 35.85 mm and a thickness of 31.50 mm. The detector was also equipped with a 0.5 mm beryllium window. The FWHM of the detector was measured to be 0.5 keV for 5.9 keV ^{55}Fe X-rays, 0.7 keV for 122 keV ^{57}Co, 1.5 keV for 1.17 MeV, and 1.6 keV for 1.30 MeV ^{60}Co gamma rays which were subsequently used to replicate the energy resolution of the detector in the simulation. The radial distance from the center of mass of the lung to the detector was set to 200 mm so that the volume of the detector did not intersect with the voxels of the phantom. In the simulations the position of the detector was changed repeatedly around the lung while keeping the radial distance fixed. All positions used in the simulations are shown in Fig. 2c) and d).

Although the dimension of the detector was determined from an X-

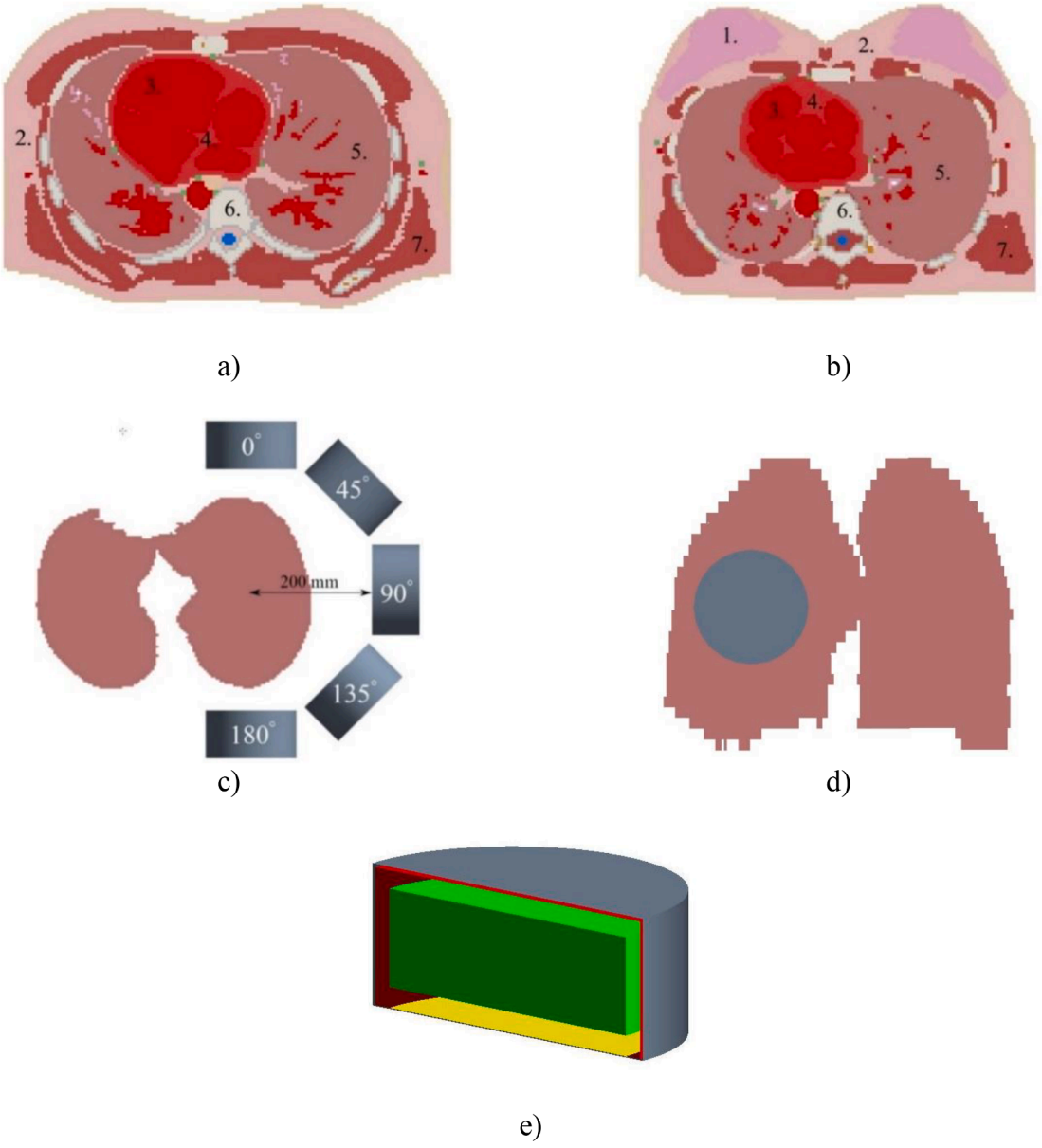

Fig. 2. a) *z*-axis chest slice of the male and b) female computational phantoms. The most common materials have been numbered 1. glandular tissue 2. adipose tissue, 3. blood 4. heart 5. lung 6. bone tissue 7. muscle tissue. c) angular positions of the detector around the right lung used in the simulations. In a similar manner, the detector can also be placed around the left lung. d) detector position in the *xz*-plane on top of the right lung. e) cross-sectional image of the HPGe detector used in the simulation. Germanium crystal (green), vacuum (red), aluminium capsule (grey), beryllium window (yellow). (For interpretation of the references to colour in this figure legend, the reader is referred to the web version of this article.)

ray image, there exists systematic uncertainty regarding the dimension of the active volume of the Ge crystal. Also, charge collection was not implemented in the simulation which would have required the electric field inside the detector to be simulated. The errors induced by Geant4 are statistical in nature and can be estimated by simulating different seeds, (the same seed will always give the same result), which can be expected to follow a normal distribution.

Therefore, the uncertainty of a single measurement is $\sqrt{N}$, where N is the number of events recorded in a single measurement. Uncertainty related to the simulation and energy deposition in the detector can be minimized by using a large sample size ($>10^6$ events), a small tracking cut (1 nm), and a high spatial resolution (small voxel size).

3. Results

In total, three simulation sets were computed in order to investigate several different aspects of the typical situations encountered in lung counting measurements. The first set corresponds to the equivalent of a 10-minute experimental measurement (based on the activities of the lungs in the physical phantom) to simulate a situation in which ^{241}Am had been inhaled (data set 1). The second data set was generated to determine the photopeak efficiency and photon transmission as a function of the energy of the emitted gamma rays (data set 2). Lastly, the position of the detector was varied around the lungs to further test the viability of the simulation package and to understand how the photon transmission through the chest wall of computational phantoms changes as a function of angular position for 59.5 keV photons, which is the characteristic gamma-ray used to identify ^{241}Am (data set 3).

Characteristic gamma and X-rays related to the decay of ^{241}Am, shown in Table 2, were used to simulate the ^{241}Am source and replicate the experimental data by emitting a single photon at a time. A total of 16 $\times$ 10^6 photons were simulated, emitted from points uniformly

Table 2
Characteristic γ and X-ray radiation related to the decay of ^{241}Am [20] where the yield is the percentage of the emitted radiation per disintegration or emission intensity.

Type	Energy (keV)	Yield (%)	Energy (keV)	Yield (%)
γ	59.54	35.90	55.56	0.018
γ	26.34	2.40	32.18	0.017
γ	33.20	0.13	42.73	0.006
γ	43.42	0.07	57.85	0.005
γ	98.97	0.02	125.30	0.004
γ	102.98	0.02	69.76	0.003
X	13.95	9.60	17.51	0.650
X	17.75	5.70	21.34	0.590
X	16.82	2.50	21.49	0.290
X	17.06	1.50	16.11	0.184
X	20.78	1.39	15.86	0.153
X	17.99	1.37	101.06	0.010
X	13.76	1.07	97.07	0.008
X	11.87	0.66	114.23	0.003
X	21.10	0.65	113.30	0.002

distributed in the lungs. The detector was placed at an angle of 0° as shown in Fig. 2a) and 2b). Simulated spectra, measured from the right side of the phantom, overlaid with the corresponding experimental spectrum are shown in Fig. 3. The experimental spectrum was background subtracted using the actual data from the background measurement with a normalization based on the measurement time. Using the 59.5 keV photopeak, the simulated spectra were scaled to correspond to the experimental spectrum. This procedure was used because the measurement geometries and materials are not identical, and the interest lies in the overall shape of the spectra and the detector response. The effect of the Ge X-ray escape peaks was also implemented in this data set by setting the Geant4 tracking cut to 1 nm [19]. Based on the measured experimental FWHM, an energy resolution function was implemented in the simulation using equations (3–5) to match the energy resolution of the detector used, which varies as a function of deposited energy.

The photopeak efficiency η and photon transmission Φ/Φ_0 as a function of photon energy were determined using the simulation package by measuring the total number of events in the photopeak after penetrating through the ICRP adult reference computational male chest wall at an angle of 0° with photon energies of 15 keV, 30 keV, 60 keV, 100 keV, 150 keV, 250 keV, 500 keV, 1000 keV, 1500 keV and 2000 keV, shown in Fig. 4a) and b). A total of 5×10^6 photons were simulated for each case. With the aim of determining the photon transmission, the simulations were repeated by setting all phantom materials to correspond to a vacuum. In this way, the total number of events in photopeak can be determined from the same irregular-shaped volume with no loss in intensity. In this case, no uncertainty in the energy deposited was introduced, and the total number of events were determined from a single channel in the spectrum. The least squares method was used to fit logaritmic functions to the data to guide the eye.

The photon transmission through the chest wall of the ICRP adult reference computational phantoms for 59.5 keV gamma rays was determined for each detector position, lung, and both male and female phantoms shown in Fig. 2c) and d). A total of 8×10^6 and 10×10^6 photons were simulated for the left and right lung, respectively, for each position. The number of counts in the photopeak was determined from a single channel in the spectrum, as again there was no need to reproduce the experimental energy resolution. The results for all the positions are shown in Fig. 5a) to d).

4. Discussion

As shown in Fig. 3, overall, the simulated spectra (data set 1) correspond well with the experimental data above 20 keV, with all the major spectral features being reproduced. The alpha decay of ^{241}Am proceeds 99.63% of the time to excited states in ^{237}Np. The de-excitation to the ground state can happen via the emission of gamma rays and/or

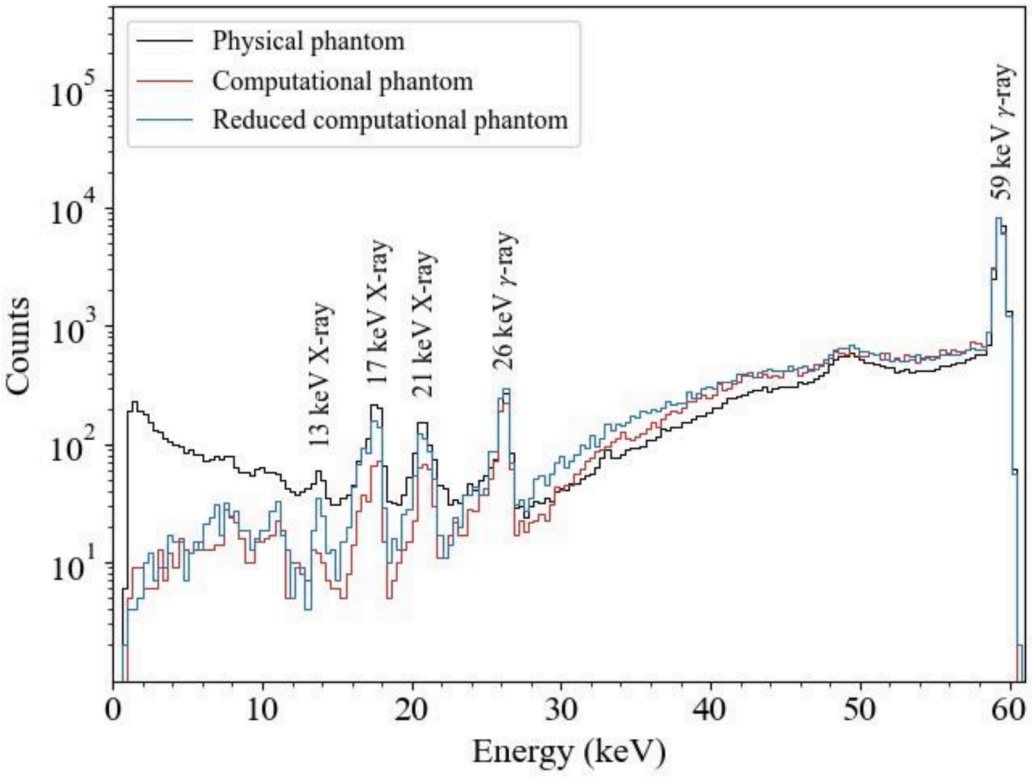

Fig. 3. Spectra of simulated and experimentally measured ^{241}Am activity inside lungs from the computational and physical phantom. In the reduced computational phantom, all materials except the lung were replaced with adipose tissue.

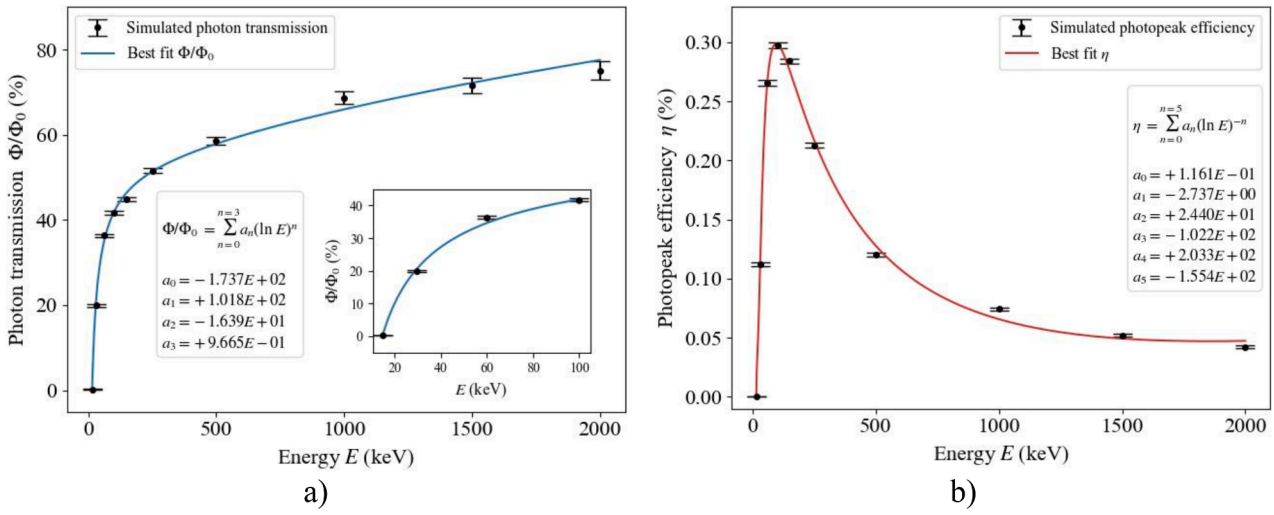

Fig. 4. a) simulated photon transmission and b) photopeak efficiency as a function of photon energy at a detector angle of 0°. Logarithmic functions were fitted to the data to guide the eye. Error bars show the standard deviation of each measurement.

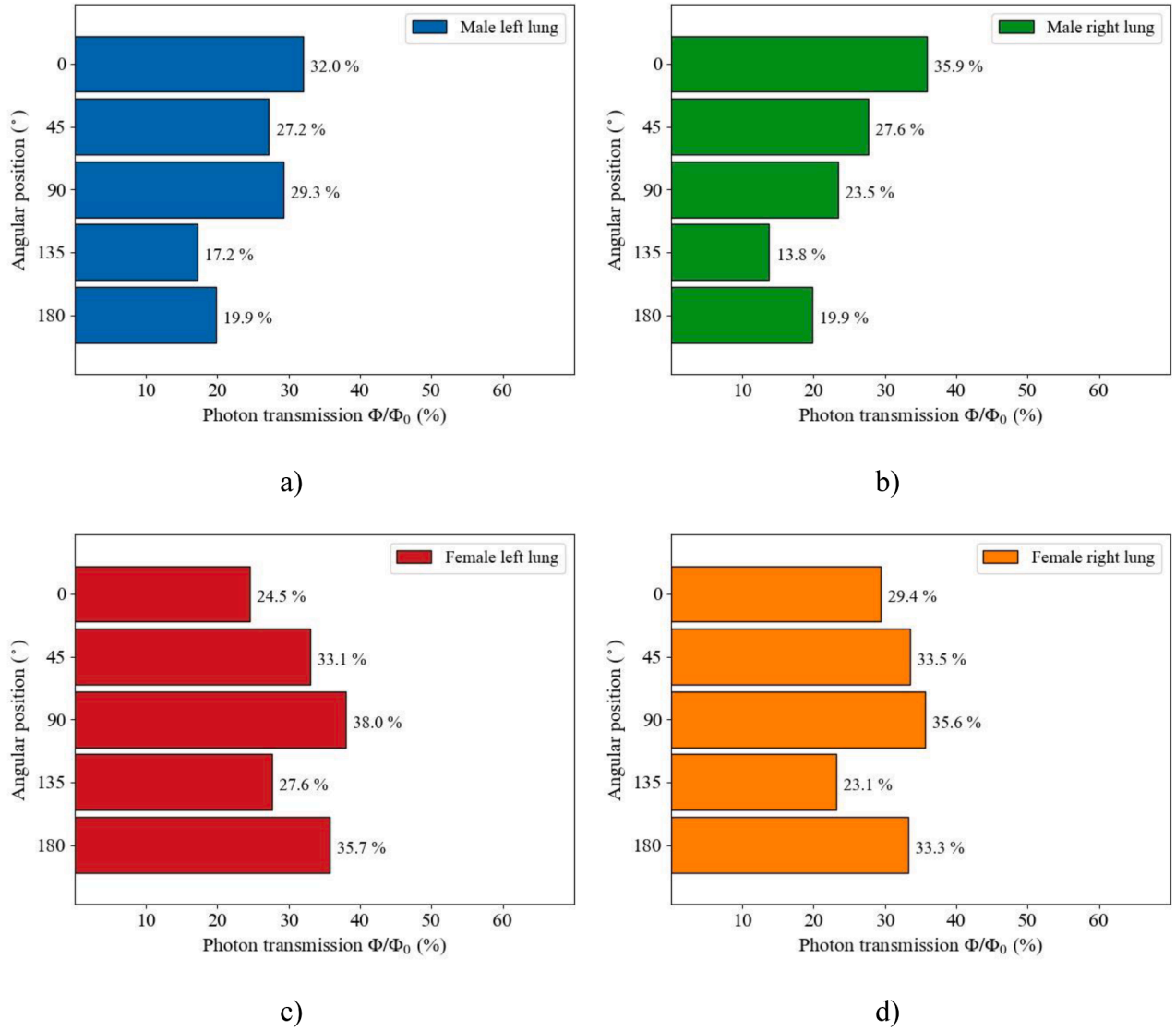

Fig. 5. Simulated 59.5 keV photon transmission as a function of the angular position of the detector. a) and b) are from the computational male phantom for each lung. Similarly, c) and d) are from the computational female phantom. Negligible small statistical errors have been omitted from the figures to aid clarity of reading.

internal conversion electrons. Thus, the decay process can also result in the emission of X-rays, Auger electrons, or both.

The most significant gamma-ray photopeaks (59 keV and 26 keV) in the simulated spectra are centered within 0.1 keV of the photopeaks in the experimentally measured spectrum as are the most prominent X-ray peaks (21 keV, 17 keV, 13 keV) determined from a Gaussian fit. The quality of the simulations can be deduced, for example, from the position and shape of the backscatter peak which is dependent on the implementation of a number of physical processes in the Geant4 libraries. A free fit to the backscatter peak in the simulated and the experimental data yields effectively identical fitting parameters (within the errors given by the fitting procedure).

Overall, the reproduction of the response of the detector and gamma-ray intensities is very good. The total count rate in the 0–100 keV region using the physical phantom was $5.1(2) \times 10^3$ cpm and $5.6(2) \times 10^3$ cpm when using the computational phantom with a relative difference of 10.0(7) % in favor of the simulated count rate. The close reproduction and slightly higher rate in the simulation comes as no surprise since the detector in the simulation is close to ideal. No dead time or dead layers were introduced and all interactions in the detector were recorded. The count rate for X-rays, however, is reduced by the more diverse materials in the computational phantom. The difference is partly caused by the composition of the computational phantom which includes high-density materials, such as bone, muscle, and cartilage tissue, that are absent in the physical phantom used to produce the experimental spectrum. This is clear when using the reduced computational phantom where all materials except the lungs were set to correspond to lower-density adipose tissue. The exact geometries of the computational and physical phantoms also differ somewhat. However, the addition of the low-background room in the simulated environment had very little impact on the final spectrum. All three factors together: non-ideal detector, differing phantom composition, and non-identical geometries between simulation and experimental measurement contribute to the differences in the low-energy part of the spectrum below 20 keV.

The photon transmission probability and photopeak efficiency were determined as a function of photon energy from data set 2. The photon transmission probability is shown in Fig. 4a). The photon transmission probability for 60 keV photons is $\Phi/\Phi_0 = 36.4(4)$ % therefore, 63.6(4) % of photons will interact with the chest wall of the phantom and cannot produce a full-energy photopeak in the final spectrum. For photons with energies above 250 keV, more than 51.6(6) % can penetrate through the chest wall unattenuated. The photopeak efficiency curve, shown in Fig. 4b), is typical for lung counting and characteristic of a germanium detector, where low-energy photons are absorbed by the chest wall and high-energy photons are more likely to go through multiple Compton scattering events instead of producing a single full-energy photopeak in the final spectrum.

To further test the phantom, the photon transmission for 59.5 keV photons was determined as a function of angular position at a fixed distance as shown in Fig. 2c). For the right lung in the male phantom, the maximum photon transmission, shown in Fig. 5b), is 35.9(4)% at an angle of 0°, which is expected since the thickness of the chest wall is minimized on top of the lung as shown in Fig. 2a). For the right lung in the female phantom, shown in Fig. 5d), the maximum is observed at an angle of 90° with 35.6(4)% due to glandular tissue as shown in Fig. 2b).

Overall, similar trends can be seen for the female and male lungs apart from the significant increase for the left lung at 90° observed for both phantoms. The probable cause for the larger photon transmission is due to the specific shape of the lung and the detail of how the emitted photons are simulated. The position of emission is randomly selected inside the lungs. Therefore, it is more likely that a photon is emitted and transmitted close to the edge of the lung since the left lung is thinner and longer than the right lung. In fact, this finding is only natural, since the left lung must make room for the heart as can be seen in Fig. 2c) and d).

5. Conclusion

A Geant4 simulation package for lung counting applications has been built from the ground up including voxelized ICRP adult reference computational phantoms. In the present work, activity due to the decay of ^{241}Am inside the lungs of the computational phantom was simulated and compared to experimental data obtained with a physical phantom made from plastic inside a low-background room at STUK. The simulated photopeak efficiency and photon transmission probability through the chest wall were determined as a function of photon energy. The photon transmission probability of 59.5 keV gamma rays characteristic to the decay of ^{241}Am decay was simulated as a function of the angular position of the detector.

The present work indicates that the results obtained from the lung counting simulation package are in good agreement with the experimental measurement. However, the results only apply to the average individual and the detector positioning needs to be evaluated carefully. In the future, the simulation package can be employed in planning future lung counting applications, through optimization of the detector design and measurement geometry. The overall outcome will be a lowering of detection limits and/or a shortening of measurement times.

Declaration of Competing Interest

The authors declare that they have no known competing financial interests or personal relationships that could have appeared to influence the work reported in this paper.

References

[1] IAEA. Assessment of occupational exposure due to intakes of radionuclides: Safety guide, Safety Standards Series No. RS-G-1.2. Vienna: International Atomic Energy Agency; 1999.
[2] ATSDR. Toxicological profile for americium. Atlanta, GA: Agency for Toxic Substances and Disease Registry: U.S. Department of Health and Human Services; 2004.
[3] ATSDR. Toxicological profile for plutonium. Atlanta, GA: Agency for Toxic Substances and Disease Registry: U.S. Department of Health and Human Services; 2010.
[4] ICRU. Direct determination of the body content of radionuclides. ICRU Report 69. J ICRU 2003;3. https://doi.org/10.1093/jicru_3.1.13.
[5] Turko J, Pillalamarri I, Jagam P. GEANT4 simulations of cosmic muon background in CEMRC BEGe lung detectors and detection sensitivity optimization of trans-uranic radionuclides. J Radiat Res Appl Sci 2020;13:111–20. https://doi.org/10.1080/16878507.2019.1711341.
[6] García Balcaza V, Camp A, Badal A, Andersson M, Almen A, Ginjaume M, et al. Fast Monte Carlo codes for occupational dosimetry in interventional radiology. Phys Med 2021;85:166–74.
[7] Arbor N, Gasteuil J, Noblet C, Moreau M, Meyer P. A GATE/Geant4 Monte Carlo toolkit for surface dose calculation in VMAT breast cancer radiotherapy. Phys Med 2019;61:112–7. https://doi.org/10.1016/j.ejmp.2019.04.012.
[8] Jan S, Benoit D, Becheva E, Carlier T, Cassol F, Descourt P, et al. GATE V6: a major enhancement of the GATE simulation platform enabling modelling of CT and radiotherapy. Phys Med Biol 2011;56(4):881–901.
[9] Kawrakow I. Accurate condensed history Monte Carlo simulation of electron transport. I. EGSnrc, the new EGS4 version. Med Phys 2000;27:485–98. https://doi.org/10.1118/1.598917.
[10] X-5 Monte Carlo Team. MCNP - A General N-Particle Transport Code, Version 5. Volume I: Overview and Theory, LA-UR-03-1987. Los Alamos National Laboratory, USA; 2003.
[11] NEA. PENELOPE 2018: A code system for Monte Carlo simulation of electron and photon transport. Paris: OECD Publishing; 2019. https://doi.org/10.1787/32da5043-en.
[12] Battistoni G, Boehlen T, Cerutti F, Chin PW, Esposito LS, Fassò A, et al. Overview of the FLUKA code. Ann Nucl Energy 2015;82:10–8.
[13] Agostinelli S, Allison J, Amako K, Apostolakis J, Araujo H, Arce P, et al. Geant4—a simulation toolkit. Nucl Instrum Methods Phys Res A 2003;506(3):250–303.
[14] ICRP. Adult reference computational phantoms. ICRP Publication 110. Ann ICRP 2009;39. https://doi.org/10.1016/j.icrp.2009.07.004.
[15] Akkoyun S, Algora A, Alikhani B, Ameil F, de Angelis G, Arnold L, et al. AGATA—advanced GAmma tracking array. Nucl Instrum Methods Phys Res A 2012;668:26–58.
[16] E. Farnea, D. Bazzacco. A Monte Carlo code for the AGATA array. LNL Annual Report 2003, LNL-INFN(REP)-202/2004 2004:158–9.
[17] Allison J, Amako K, Apostolakis J, Arce P, Asai M, Aso T, et al. Recent developments in Geant4. Nucl Instrum Methods Phys Res A 2016;835:186–225.

[18] Guatelli S, Cutajar D, Oborn B, Rosenfeld AB, Rosenfeld A, Kron T, et al. Introduction to the Geant4 simulation toolkit. In: AIP Conference Proceedings; 2011. p. 303–22. https://doi.org/10.1063/1.3576174.
[19] Georgali E, Patronis N, Anastasiadis A, Axiotis M, Harissopulos S, Karfopoulos K, et al. Using GEANT4 Monte Carlo simulations to resolve low energy γ-ray spectra: The study of $^{164}Ho^{g+m}$ decay using a broad energy HPGe detector. Nucl Instrum Methods Phys Res A 2021;985:164711. https://doi.org/10.1016/j.nima.2020.164711.
[20] Nesaraja CD. Nuclear Data Sheets for A = 241. Nucl Data Sheets 2015;130:183–252. https://doi.org/10.1016/j.nds.2015.11.004.